Tunneling and charging effects in discontinuous superparamagnetic $Ni_{81}Fe_{19}/Al_2O_3$ multilayers

R. Bručas, M. Hanson, and P. Apell
Department of Applied Physics, Chalmers University of Technology, SE-412 96 Göteborg, Sweden

P. Nordblad
Department of Engineering Sciences, Uppsala University, P.O. Box 534, SE-751 21 Uppsala, Sweden

R. Gunnarsson
Department of Microtechnology and Nanoscience, Chalmers University of Technology, SE-412 96 Göteborg, Sweden and HLK, Jönköping University, SE-551 11 Jönköping, Sweden

B. Hjörvarsson
Department of Physics and Materials Science, Uppsala University, P.O. Box 530, SE-751 21 Uppsala, Sweden
(Received 10 November 2009; revised manuscript received 17 March 2010; published 29 June 2010)

The magnetic and transport properties of films based on discontinuous layers of $Ni_{81}Fe_{19}$ (Py) embedded in Al_2O_3 were investigated. In films with nominal Py thicknesses 6 and 8 Å superparamagnetic particles with median diameters $D_{med}=2.8$ and 3.1 nm and distribution widths $\sigma_D=1.2$ and 1.3 nm were formed. Current voltage (IU) curves were measured with the current perpendicular to the film plane. The analyses show that the charge transport occurs via tunneling; with the charging energy supplied by thermal fluctuations at high temperature, $T \geq 100$ K, and by the electric field at low temperature, $T<10$ K. The separation of the two regimes allows independent estimates of the mean charging energy $\langle E_C \rangle \approx 40$ meV for both samples; from the resistance R versus T analyzed in an effective-medium model at high temperature and from I versus U at 4 K. In order to obtain a consistent description of the transport properties, the size distributions must be included to account for the deviation from the single size behavior $R \sim \exp(E_C/k_BT)$ at high T. The scaling parameter in the relation $I \propto (\frac{U}{U_{th}}-1)^{\gamma}$, where U_{th} is the threshold for conduction, is estimated to $\gamma \approx 2$ at 4 K. The superparamagnetic relaxation of the particles becomes blocked below a temperature $T \approx 20$ K respective 30 K for 6 and 8 Å. The magnetic field (B) dependence of the resistance $R(B)$ displays a single maximum of the ratio $MR=[R(B)-R(2\ T)]/R(2\ T)$ in zero field at room temperature and a characteristic splitting of the peak at 4 K, attributed to the blocking. The maxima, ≈0.9% for 6 Å and 1.1% for 8 Å, are positioned at fields about a factor of two to three higher than the coercive fields of the samples.

DOI: 10.1103/PhysRevB.81.224437 PACS number(s): 73.21.Ac, 73.40.Gk, 73.43.Qt, 75.47.−m

I. INTRODUCTION

The field of spintronics explores the interplay of spin-polarized conduction electrons and magnetization which leads to, e.g., giant magnetoresistance (MR) (Refs. 1–4) or tunnel MR (TMR) (Refs. 5–7) effects. Whereas such effects already find technological applications (magnetoresistive read heads and nonvolatile magnetic memories) much of the underlying physics remains to be explored, especially in the few-nanometer-scale magnetic structures. There discrete energy levels and large charging energies together with strong temperature and field dependences of the magnetization play important roles in spin and charge transport.

The correlation between superparamagnetism and transport properties was investigated 1972 by Gittleman *et al.*[8] in granular Ni/SiO_2. More recent investigations of different ferromagnetic (Fe, Ni, Co, and their alloys) nanogranules revealed a remarkable enhancement of the TMR.[9–13] This stimulated further investigations of spin-dependent transport in systems comprising metallic nanoparticles separated by insulating barriers, in particular, in the regime where the electron transport is suppressed by the Coulomb blockade due to charging effects.[14]

Both the size of and the distance between magnetic particles can be varied independently in discontinuous multilayers. We use this approach to explore the influence of particle size on the conductivity of discontinuous layers of Py (permalloy, $Ni_{81}Fe_{19}$) embedded in Al_2O_3 in the vicinity of the superparamagnetic limit. The system with magnetically soft Py, with high permeability, high saturation magnetization, and low coercivity in combination with Al_2O_3 with high resistivity may also find use in high-frequency devices.[15] In our recent work on the magnetic and transport properties in $Ni_{81}Fe_{19}/Al_2O_3$ multilayers,[16,17] we found that the percolation both in the conductive and magnetic behavior occurs for a nominal Py layer thickness t_{Py} in the range $10 \leq t_{Py} \leq 12$ Å. The transport properties were measured with the current in the plane of the film (CIP geometry) where no clear-cut charging effects were observed. In order to study these effects further, in this work we choose a configuration with the current perpendicular to the plane of the film (CPP geometry). Since the number of particles in a current path is then reduced compared to that in the CIP geometry, being on the order of 10^6, the character of the events in the transport process will be easier to distinguish.

II. EXPERIMENTS

The multilayers were prepared under identical conditions as in our earlier study[16] by dc and rf sputtering of Py and

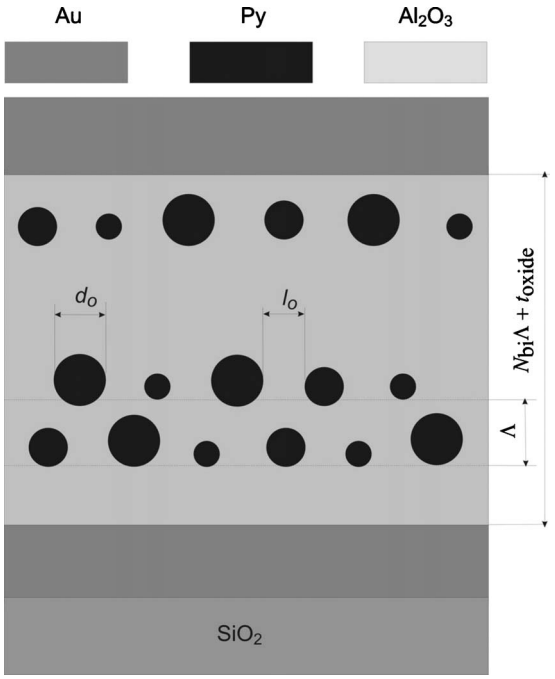

FIG. 1. Schematic representation of the cross section of a typical discontinuous $Ni_{81}Fe_{19}/Al_2O_3$ multilayer. $\Lambda = t_{Py} + t_{oxide}$ is the period of the layered structure with t_{Py} and t_{oxide} being the nominal thicknesses of the permalloy and aluminum oxide layers, respectively. N_{bi} is the total number of bilayers in a film.

Al_2O_3, respectively. The deposition rates were controlled by a quartz crystal microbalance precisely calibrated against thickness measurements using x-ray reflectivity. A series of samples were made with a nominal thickness of the Al_2O_3 layers $t_{oxide}=14$, 16, or 18 Å and the nominal thickness t_{Py} of the Py layers between 6 and 16 Å. By nominal thickness we mean the thickness a given amount of deposited material would yield provided it was evenly distributed in a layer. In the following we use these notations of the nominal thickness to identify the samples. The number of bilayers N_{bi} was varied from 8 to 26 in order to keep the total amount of magnetic material in a sample constant. Al_2O_3 grows amorphous at room temperature, and Py grows polycrystalline. Due to the large difference in surface energies of the metal and the insulator, Py does not wet Al_2O_3, thus supporting a perfect Volmer-Weber growth mode.[18] Then the film growth goes through three main stages as t_{Py} increases: nucleation of small clusters, formation of islands, and development of continuous films.

We present results for two samples with $t_{oxide}=16$ Å, with $t_{Py}=6$ Å, $N_{bi}=26$ and $t_{Py}=8$ Å, $N_{bi}=20$, respectively. These permalloy thicknesses are well below the percolation limit,[16] thus each sample forms a periodic metal insulator with discontinuous Py layers embedded in Al_2O_3, cf. Fig. 1. Here d_0 and l_0 denote the mean size of and the mean distance between the particles, respectively.

For resistance measurements 20 μm $\times$ 20 μm junctions sandwiched between Au electrodes were prepared using multistep optical lithography and ion-beam milling. The measurements were made in a He-flow cryostat with a superconducting magnet. The voltage U was measured as the bias current I was varied in the range ± 100 μA in steps of 0.5 μA, and the temperature was varied in the range $4 \leq T \leq 300$ K. The magnetic field dependence was measured at a constant bias current $I=100$ μA with the magnetic field $-5 \leq B \leq 5$ T applied in the film plane. The measurements at low temperature were made after cooling in zero field. Rectangular samples were cut for magnetization measurements with an alternating gradient magnetometer (AGM) at room temperature and a superconducting quantum interference device (SQUID) magnetometer in the range $5 \leq T \leq 300$ K. Field-cooled (FC), zero-FC (ZFC), and thermoremanent (TRM) magnetization were measured as a function of temperature in an applied field of 2 mT. All magnetic measurements were made with the field applied in the plane of the film and the hysteresis curves were corrected for diamagnetic backgrounds.

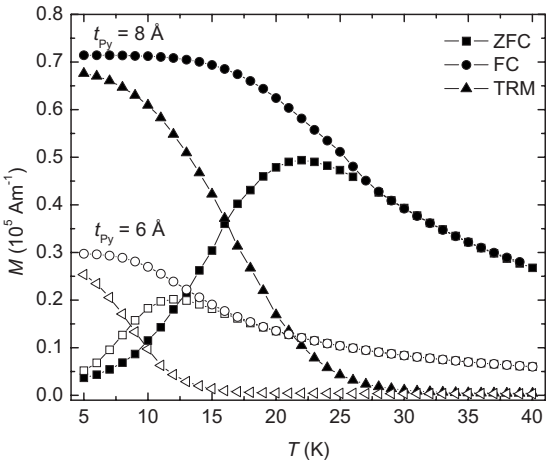

FIG. 2. Magnetization vs temperature measured in an applied field of 2 mT using zero-FC (ZFC), FC, and thermoremanent (TRM) magnetization protocols. The open symbols show the sample with $t_{Py}=6$ Å and the filled symbols the sample with $t_{Py}=8$ Å.

III. RESULTS

A. Magnetic properties

The ZFC, FC, and TRM curves are shown in Fig. 2. For $t_{Py}=6$ Å the characteristic features are: the ZFC curve has a broad maximum at $T \approx 12$ K, the ZFC and FC curves coincide down to 18 K and the TRM approaches zero above 20 K. For $t_{Py}=8$ Å, the thermal blocking is shifted to higher temperatures: the maximum in the ZFC field is at $T \approx 22$ K, the ZFC and FC curves coalesce and the TRM approaches zero above 30 K.

The transition from superparamagnetism to thermal blocking is evidenced also when comparing the magnetic hysteresis loops measured at room temperature and at 5 K, see Fig. 3. At 5 K the magnetization shows hysteretic behavior with a relative remanence $M_r \approx 0.5 M_{max}$ and a coercivity $B_c \approx 50$ mT for the sample with $t_{Py}=6$ Å. The corresponding values for $t_{Py}=8$ Å are $M_r \approx 0.6 M_{max}$ and $B_c \approx 60$ mT. Due to the uncertainty in the diamagnetic corrections, the absolute values of the saturation magnetization and the rela-

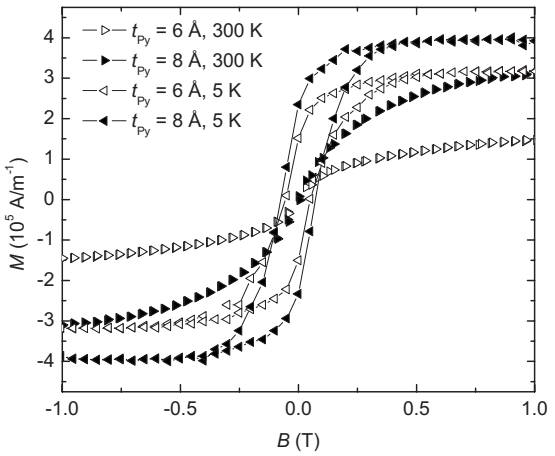

FIG. 3. Magnetization vs applied magnetic field curves measured at 300 K (AGM) and 5 K (SQUID) with the field applied in the film plane. The permalloy layer thickness and the temperature are indicated in the figure.

tive remanence are considered to be rough estimates here. The coercivities are, however, well determined.

In the superparamagnetic regime, well above the blocking temperatures and where the interparticle dipolar interaction is weak compared to the thermal energy, the magnetization can be described by a superposition of Langevin contributions from particles having a size distribution with median diameter D_{med} and a distribution width σ_{D}.[19] Figure 4 shows such Langevin fits in the field interval 0–1 T of the M versus B curves measured at 100 K for $t_{\mathrm{Py}}=6$ Å, and at 300 K for $t_{\mathrm{Py}}=8$ Å. Using the value 7.12×10^5 Am^{-1} for the intrinsic magnetization of permalloy these fits yield $D_{\mathrm{med}}=2.8$ nm and 3.1 nm and $\sigma_{\mathrm{D}}=1.2$ and 1.3, respectively. Adopting these particle sizes and taking the corresponding volume concentrations of Py, $c=6/22$ and 8/24, we obtain dipolar interaction temperatures of about 11 K for the 6 Å film and 18 K for the 8 Å film. The fits are thus made at temperatures where the influence of dipolar interactions is weak. The stability of the derived particle sizes was checked by performing Langevin fits of all M versus B data measured at high temperatures using varying field intervals; all fits yielding particles sizes within $D_{\mathrm{med}}\pm0.5$ nm of those derived from the fits in Fig. 4. An Arrhenius law $\tau_{\mathrm{exp}}=\tau_0\exp(KV/k_{\mathrm{B}}T)$ can be used to estimate the anisotropy constant K of the particles. τ_{exp} and τ_0 are the experimental and intrinsic fluctuation times, V the particle volume, and k_{B} the Boltzmann constant. With the maxima of the ZFC curves taken as the blocking temperatures for $\tau_{\mathrm{exp}}=100$ s and $\tau_0=10^{-10}$ s, the values $K\approx5\times10^5$ J m^{-3} and 7×10^5 J m^{-3} are obtained for 6 Å and 8 Å, respectively. Magnetic anisotropy of this order of magnitude leads to deviations from the Langevin behavior of small particles to a varying degree for different fields.[20,21] An estimate the effect of anisotropy on the derived size distributions would require a wider range of fields than in the present investigation, in order to determine the saturation magnetization of the samples.

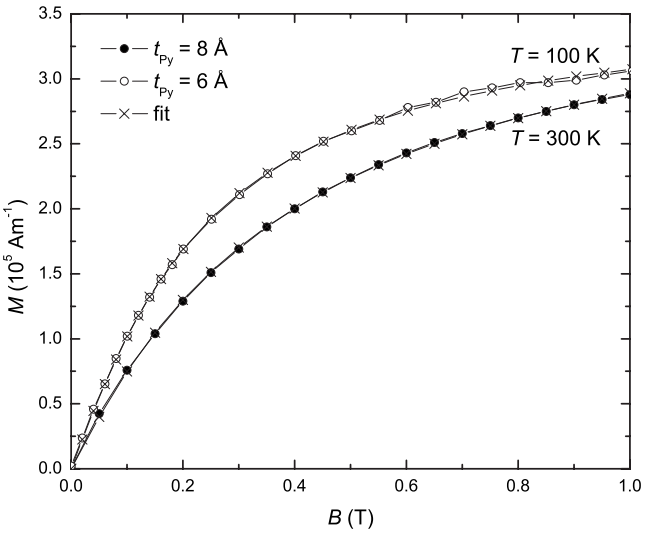

FIG. 4. Fit of Langevin functions over a size distribution to the magnetization curves of the samples with $t_{\mathrm{Py}}=6$ and 8 Å, as noted in the figure. The measurements were made at the temperatures 100 and 300 K, well above the respective blocking temperature of the samples.

B. Transport properties

In the following we analyze first the resistance at high temperatures, where the voltage dependence is negligible, and then the voltage dependence of the current at low temperature, where the temperature dependence is weak, cf. Fig. 5. Finally the magnetic field dependence is described.

1. Temperature dependence of the resistance at high temperature

Both samples display a strong temperature dependence of the resistance with a negative temperature coefficient ($dR/dT<0$) from room temperature down to below about 10 K for 6 Å and 20 K for 8 Å. In the range from room temperature to $T\approx100$ K the current I depends linearly on the applied voltage for bias voltages up to $U=3$ V, cf. Figs. 5(a) and 5(b). Thus, in the high-temperature range the conductance is independent on electric field. As discussed already in 1962 by Neugebauer and Webb[22] the charge transfer between the islands of an ultrathin metal film occurs by tunneling when the separation between the islands is on the order of a few nanometers. From the gap in the low-temperature IU curves we know that the particles in our films are electrically isolated, see Figs. 5(c) and 5(d) and discussion below. In sufficiently large magnetic grains the electronic level splitting at the Fermi level is small. Then, at ambient temperatures the conduction is governed by charge carriers excited to a level E_{C} above the Fermi energy that tunnel from one neutral particle to another. To create a charge e in a single, initially neutral particle of linear extension d requires an electrostatic energy of magnitude,

$$E_{\mathrm{C}}\propto\frac{e^2}{d}. \tag{1}$$

The negative temperature coefficient indicates a thermally activated charging process, thus suggesting a conductivity σ depending on the number n of charged (or excited) particles in thermal equilibrium,

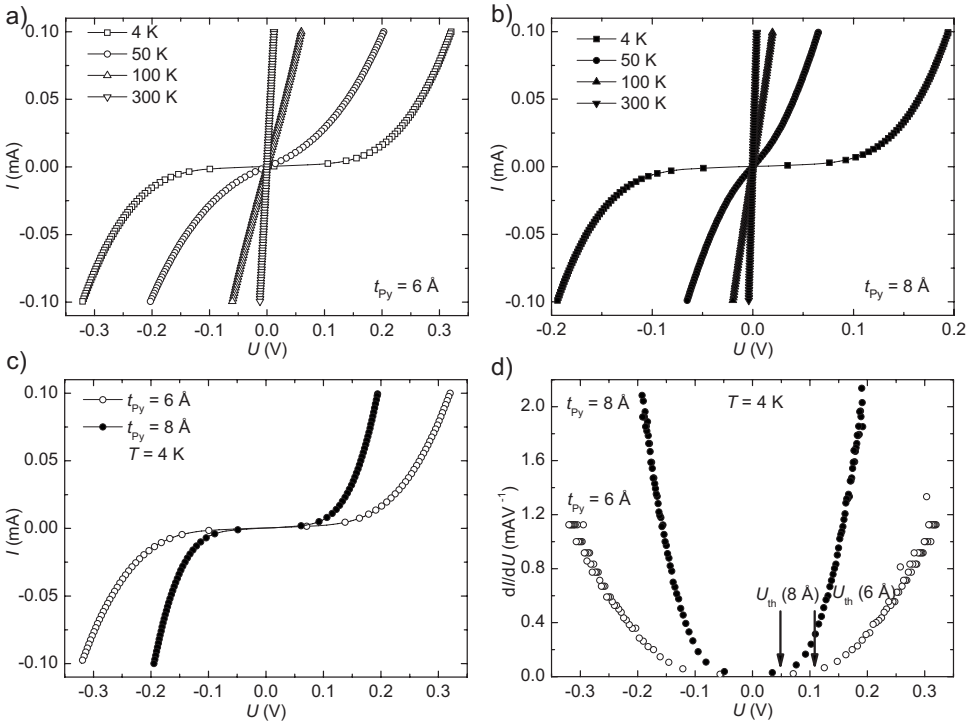

FIG. 5. Current vs voltage for the $Ni_{81}Fe_{19}/Al_2O_3$ multilayers with permalloy layer thickness in (a) t_{Py}=6 Å and in (b) t_{Py}=8 Å. The measurements were made at temperatures in the range $2 \leq T \leq 300$ K, as noted in the figure. (c) and (d) show I vs U and (dI/dU) vs U for the two samples at 4 K.

$$n = Ne^{-E_C/k_B T}. \tag{2}$$

Here N is the total number of particles in a sample. To obtain the best possible accuracy we determined the resistance from the slopes of the IU curves in the high-temperature range, where the current-voltage relations are linear. In Fig. 6 the logarithm of these values are plotted versus the inverse temperature. The curves deviate from straight lines due to the spread in particle sizes as we will now show.

With the conductivity proportional to the number of excited grains, according to Eq. (2) above, we can write for the logarithm of the resistance,

$$\ln R = \text{const} - \ln\langle e^{-E_C(d)/k_B T}\rangle, \tag{3}$$

where $\langle\ \rangle$ denotes an average over the log-normal grain size distribution. Since we are interested in the first nonvanishing correction to the dependence on $1/T$, i.e., second order in E_C/T, we expand the exponent as well as the logarithm in Eq. (3) above and write

$$\ln R = \text{const} + \left\langle \frac{E_C(d)}{k_B T} \right\rangle - \frac{1}{2}\left(\frac{\Delta E_C}{k_B T}\right)^2 \cdots, \tag{4}$$

$\langle E_C(d)\rangle$ is the average charging energy and ΔE_C is the fluctuation in charging energy according to

$$\Delta E_C^2 \equiv \langle E_C^2(d)\rangle - \langle E_C(d)\rangle^2. \tag{5}$$

In this way the curvature of the resistance curve with respect to the inverse temperature has information about the size distribution of the particles. Based on a log-normal distribution one can show that for $E_C(d) \propto 1/d$,

$$\frac{\Delta E_C}{\langle E_C(d)\rangle} = \sqrt{e^{\ln^2 \sigma_D} - 1}. \tag{6}$$

In other words, the fluctuations in charging energy are directly related to the logarithm of the geometric standard deviation for the size distribution. Figure 6 shows that a second-order relation in $1/T$ fits well to the experimental data. These fits yield estimates of $\langle E_C(d)\rangle \approx 40.1$ and 39.4 meV and $\Delta E_C = 15.7$ and 15.6 meV for the samples with 6 Å and 8 Å thick permalloy layers, respectively. The differences between the samples fall within the uncertainty of the size distributions of respective samples. With the estimated values we get the ratios in Eq. (6) as 0.39/0.40 while the right-

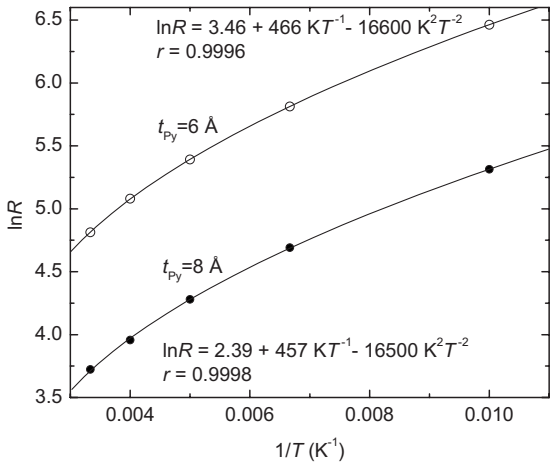

FIG. 6. The logarithm of the resistance of the 6 and 8 Å samples plotted versus the inverse temperature in the range $100 \leq T \leq 300$ K. The equations and the curves represent fits of a relation of second order in $1/T$. r is the regression coefficient.

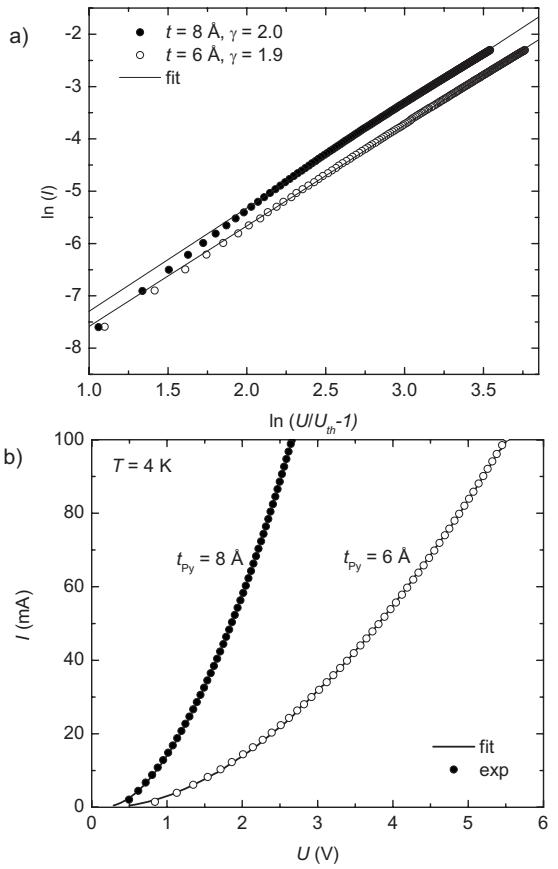

FIG. 7. (a) shows a plot representing the logarithm of the relation (7) for the $Ni_{81}Fe_{19}/Al_2O_3$ multilayers with 6 and 8 Å thick Py layers, as noted in the figure. The exponent γ is obtained from the slope of the linear fit. In (b) the *IU* curves are plotted together with fits of a second-order polynomial to the experimental points.

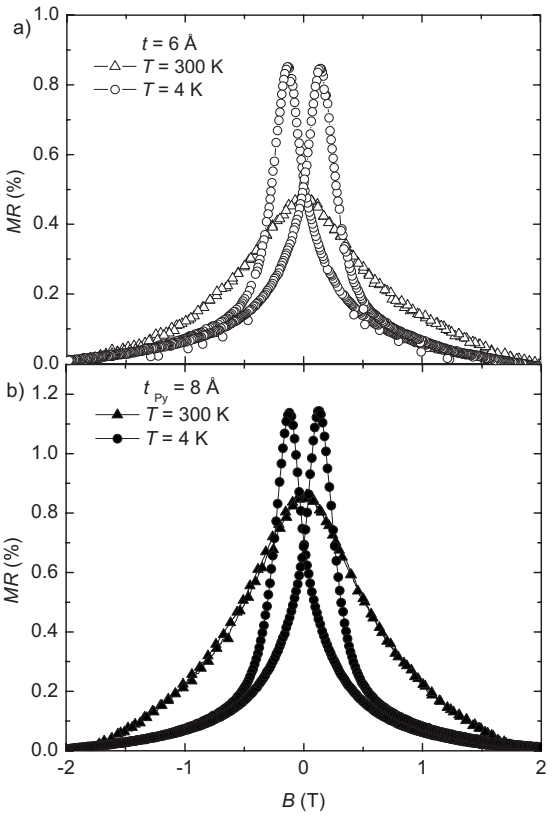

FIG. 8. Magnetic field dependence of the resistance ratio MR $=[R(B)-R(2\ \mathrm{T})]/R(2\ \mathrm{T})$ for the $Ni_{81}Fe_{19}/Al_2O_3$ multilayers with 6 and 8 Å thick Py layers, as noted in the figure. The measurements were made at room temperature and 4 K in a CPP geometry.

hand side is 0.18/0.27 as deduced from the size distributions ($\sigma_D=1.2/1.3$). Considering the simplicity of the model analysis the agreement is reasonable.

2. Voltage dependence of the current at low temperature

Below 100 K the *IU* curves get progressively more nonlinear with decreasing temperature, see Figs. 5(a) and 5(b). One can notice that in order to generate a current between the nanoparticles below 20 K a finite voltage is necessary. This energy gap shows that the particles are electrically isolated. A threshold voltage for conduction was estimated from the differential conductance (dI/dU) at 4 K, see Fig. 5(d), yielding $U_{th}\approx 0.125$ V for $t_{Py}=6$ Å and 0.075 V for $t_{Py}=8$ Å. Above the threshold the voltage dependence of the current is governed by the number of available paths for the charge transport. A relation of the form,

$$I \propto \left(\frac{U}{U_{th}} - 1\right)^{\gamma} \tag{7}$$

was predicted for a uniform array of islands with γ being a scaling parameter depending on the array dimensionality.[23] In Fig. 7(a) the logarithm of Eq. (7) is fitted to the experimental data. The best fit yields the values $\gamma\approx 1.9$ and 2.0 of the scaling parameter for 6 Å and 8 Å, respectively. The threshold U_{th} is defined as the voltage when the current exceeds a measurable value above about 10^{-8} A corresponding to a certain number of current paths that are open. Since the tunneling occurs between particles with a size distribution, there is a certain range of voltages, $U_{th}<U<U_o$ where an increasing number of channels become available as the energy of the electric field becomes sufficient to supply the charging energy of the smaller particles. If we assume that the high-field scaling parameter is 2 and fit a second-order polynomial to the *IU* curves we obtain an estimate of U_o from the voltage where the experimental points deviate from the fit, see Fig. 7(b). This yields $U_o\approx 1.1$ V for $t_{Py}=6$ Å and about 0.8 V for $t_{Py}=8$ Å. A voltage U_o over the sample corresponds to a voltage $\delta U=U_o/(N_{bi}+n)$ between two consecutive layers of permalloy particles. Here $n=t_{oxide}/(t_{Py}+t_{oxide})$, cf. Fig. 1. With $N_{bi}=26$ and 20 this yields $\delta U\approx 41$ mV for 6 Å and 39 mV for 8 Å.

3. Magnetic field dependence of the resistance

Figure 8 shows the resistance ratio MR$=[R(B)-R(2\ \mathrm{T})]/R(2\ \mathrm{T})$ versus field at 4 and 300 K. Here $R(2\ \mathrm{T})$ is the resistance measured in $B=2$ T. Both samples have similar characteristic features, slightly differing quantitatively. The 6 Å sample shows a maximum of $MR_{max}\approx 0.50\%$ in zero field at 300 K and a resistance smoothly decreasing with increasing magnetic field. At 4 K two well-

separated maxima are developed: $MR_{max} \approx 0.87\%$ at $|B_m| \approx 150$ mT. This field is about a factor of three higher than the coercive field $B_c \approx 50$ mT obtained in the hysteresis loop, cf. Fig. 3. For 8 Å the room-temperature maximum is 0.88%. At 4 K the $MR_{max} \approx 1.16\%$ occurs at $|B_m| \approx 125$ mT, about a factor of two higher than the coercive field of 60 mT, cf. Fig. 3.

IV. DISCUSSION

A. Structure and magnetic properties

The discontinuous multilayers of $Ni_{81}Fe_{19}/Al_2O_3$ investigated in this work have nominal metal thicknesses well below the percolation threshold $10 \leq t_{Py} \leq 12$ Å.[16] The particle sizes extracted from the magnetic data, diameter 2.8 and 3.1 nm, may appear large compared to the nominal Py thicknesses 6 and 8 Å. The sizes are, however, compatible with the Volmer-Weber growth[18] and they compare well with the transmission electron microscopy image of the 8 Å sample in an earlier investigation,[16] where four particles seem at average to require about 20 nm length in each Py layer. One can also note that the relation between deposited metal film thicknesses and particle sizes is comparable to that found in other systems. For example; Morawe and Zabel[24] found a percolation threshold for Co layers on sapphire in the range 1.5–2.5 nm and Fettar *et al.*[25] obtained mean particle diameters of 2.0, 3.7, and 4.8 nm when they deposited single Co layers of respective thicknesses 0.4, 0.7, and 1 nm in Al_2O_3.

The change in the magnetic properties with increased nominal magnetic layer thickness of our multilayers accords earlier findings that thin layers result in small particle size and weak interparticle interaction (as in the current investigation) and thicker metal layers introduce collective behavior and finally a percolating ferromagnetic state. This evolution, including a tentative phase diagram, was demonstrated by Kleemann *et al.*[26] in a study of $Co_{80}Fe_{20}/Al_2O_3$ discontinuous metal-insulator multilayers (DMIM).

B. Charging energy and interactions

Whereas many studies were made on spin-dependent tunneling and magnetoresistance in DMIM, e.g.,[27–34] only few applied the CPP configuration, where the gap in the tunneling conductance can be observed at low temperature. Sankar *et al.*[27] measured the transport properties of $CoFe/HfO_2$ multilayers with 20 bilayers. For a 15 nm CoFe layer they determined a charging energy of 15 meV per tunnel barrier from the conductivity gap at 10 K. A fit of the resistance to a T dependence $\rho \sim \exp(E_C/k_BT)$ yielded a value of 20 meV in the high-temperature regime, $T \geq 180$ K. The particle sizes were estimated to be slightly larger, 3.5 nm, than in our $Ni_{81}Fe_{19}/Al_2O_3$ multilayers, and thus a lower charging energy could be expected. The size distribution was not considered in the evaluation by Sankar *et al.* We showed that to obtain a consistent description of the transport properties, the size distribution must be included to account for the deviation from the single size $\exp(E_C/k_BT)$ behavior at high temperatures. The smallest Py particles we investigated in the CIP configuration had a nominal permalloy layer thickness of 10 Å. For that sample an energy barrier for conduction of 20 meV was estimated from the temperature dependence of the resistance.[16] Those results support the trend of the charging energy decreasing with increasing particle size.

A further aspect to consider is that a charge on a particle induces a polarization in the dielectric matrix as well as the surrounding metal particles and the energy of the whole system changes. Neugebauer and Webb[22] neglected the interactions between the charges. It is not straightforward to calculate an effective capacitance of a metal particle in a granular system and different approximations were applied in other work. For example, Hill[35] included the interactions between nearest neighbors of identical particles with radius r, separated by a barrier s and arrived at a change in the potential,

$$\delta E_0 = \frac{e^2}{\epsilon\epsilon_0} \frac{r+s}{r(2r+s)}. \tag{8}$$

Here ϵ and ϵ_0 are the relative permittivity of the matrix and the permittivity of vacuum, respectively. Expressions involving slightly different combinations of the same parameters can be found in the papers by Sheng and Abeles,[36] Ruggiero and Barner,[37] or Black *et al.*[11] We applied these expressions and integrated over the particle size distributions to estimate the number of particles charged by thermal excitations and found that it is possible to obtain reasonable fits to the curvature of temperature-dependent resistance. We concluded, however, that small changes in the relations between the geometric parameters lead to large variations in the extracted physical properties of the system.

As an alternative to previous approaches we take a more general view on the charging energy in order to include effects from a larger surrounding than nearest-neighbor particles in terms of an effective medium. We write

$$E_C(d) = \frac{e^2}{2C} = \frac{e^2}{4\pi\epsilon_{eff}\epsilon_0} \frac{1}{d}, \tag{9}$$

where C is the capacitance of a particle with diameter d. ϵ_{eff} is the relative dielectric function of the effective-medium screening the charges in the system with a mixture of aluminum oxide and permalloy dielectric properties. Taking an ensemble average over the log-normal particle size distribution and using that $\langle d \rangle / \langle 1/d \rangle = D_{med}^2$ and $\langle d \rangle = D_{med} \exp(\frac{1}{2} \ln^2 \sigma_D)$ we get,

$$\langle E_C(d) \rangle = \frac{e^2}{4\pi\epsilon_{eff}\epsilon_0 D_{med} e^{-1/2 \ln^2 \sigma_D}}. \tag{10}$$

Notice that the effective size entering the charging energy is smaller than the median diameter. Inserting the experimentally determined values for D_{med}, σ_D, and $\langle E_C(d) \rangle$ we get ϵ_{eff} about 13 and 12 for $t_{Py}=6$ Å and 8 Å, respectively. These results, describing the effective dielectric function of the medium surrounding a permalloy particle, can be related to the dielectric functions of the permalloy particles ϵ_{Py} and the aluminum oxide matrix ϵ_{ox}, the filling factor c of permalloy and the shape of the particles described by a depolarization factor L. If we assume the static (dc) value of ϵ_{Py} to be much higher than that of $\epsilon_{ox} \approx 8$ (Ref. 38) the effective dielectric function in the Maxwell Garnett theory[39] becomes

$$\epsilon_{\text{eff}} \approx \left(1 + \frac{c}{L}\right)\epsilon_{\text{ox}}, \tag{11}$$

provided c is small. Inserting the above derived values of ϵ_{eff} together with $c=3/11$ for 6 Å and $c=1/3$ for 8 Å, in Eq. (11) we deduce a depolarization factor of 0.4 for the particles in the 6 Å film and 0.6 for those in the 8 Å film. That indicates that within this model the particles are rather spherical for 6 Å ($L=1/3$ for spheres) and more oblate for 8 Å ($1/3<L<1$, where 1 corresponds to a sheet).

C. Scaling parameters in *IU* curves

It is not obvious what conclusions one can draw from the scaling parameter γ in Eq. (7). One aspect is that it may be related to the dimensionality of the system. As derived analytically by Middleton and Wingreen[23] the values of the scaling parameter are 1 and 5/3 for one dimension and two dimension (2D), respectively. In a numerical simulation they obtained $\gamma=2$ for 2D. Gupta and Sen[40] developed a model comprising metallic particles, with Ohmic conductivity, in an insulating matrix where conduction between nearest-neighbor particles occurs via tunneling over barriers. Calculations for the 2D case showed that the scaling parameter is determined by the filling factor together with the number of open tunneling paths, which in turn depends on the applied electric field. A minimum of $\gamma \equiv 2$ was obtained at percolation. Analyses of the scaling parameter were applied also in other experimental work. Rimberg *et al.*[41] measured the *IU* characteristics of one- and two-dimensional arrays of metal islands linked by small tunnel junctions. They found $\gamma=1.36$ and 1.80 for the two cases, respectively. Lebreton *et al.*[42] performed experiments on colloidal films of Pd particles deposited between electrodes on a sample surface. From the *IU* curves of the samples they derived $\gamma=2.1$ for a 2D sample and $\gamma=3.5$ for a three-dimensional (3D) sample. Similar devices of Co particles prepared by Black *et al.*[11] yielded $2.2<\gamma<2.7$. Tan *et al.*[43] present a variety of γ values for superlattices of CoFe particles.[43] Together, theoretical models and experiments show that the structure and dimensionality of the metal particle system strongly influence the deduced γ values. About our system we can say that the value obtained from the *IU* curves $\gamma \approx 2$ has been found for the 2D case in theoretical models. We found no corresponding calculations for the 3D case.

D. Magnetoresistance

Among the plethora of magnetoresistive behavior observed in DMIMs salient features that are often discussed are the absolute values of the MR maximum and whether a single peak or a split maximum is present. A single maximum at room temperature, which becomes split as the temperature decreases indicates that the hysteretic behavior is related to the blocking of superparamagnetic relaxation in small particles. We observed this both in the CIP and CPP configurations but with a better resolution for CPP. One reason for this is that the low-temperature resistance of the $Ni_{81}Fe_{19}/Al_2O_3$ multilayers is lower in the CPP configuration and samples with thinner permalloy layers could be investigated. The maximum of the measured decrease in the resistance in a magnetic field was on the order of 1% in both samples. Factors that influence the absolute values of the magnetoresistance are on one hand the structural properties such as the particle sizes, the number of accessible current paths and the number of tunneling steps in each path and on the other hand the material properties such as the degree of spin polarization and the magnetic anisotropy of the ferromagnetic particles. Examples of other devices where the magnetoresistance ratio MR was measured are given by: Schelp *et al.*[9] studied single layers of 2.5 nm Co particles embedded in Al_2O_3 between Co electrodes yielding values of MR up to 10%, with Co particles, Yakushiji *et al.*[12] studied a nanobridge of a granular CoAlO film with Co particle diameters about 2.5 nm and MR about 35%, and Varalda *et al.*[44] studied a granular film of Co clusters with diameters 3–4 nm in TiO_2 with MR of about 2–3 %. In these examples the MR values are higher than in our permalloy/Al_2O_3 multilayers due to the higher anisotropy and spin polarization in Co particles and/or to a lower number of tunneling steps through the samples.

As for our multilayers, a shift between the field at the MR maxima and the coercivity of the samples was observed also by Varalda *et al.*,[44] for temperatures in the Coulomb-blockade regime. It is not straightforward to give account for the relation between the fields for this complex system. This would require a separate investigation, for instance, of how the number of open tunneling paths depends on field for samples with a varying number of layers and particle size distributions.

A fundamental question is how the magnetoresistance is affected when entering the Coulomb-blockade regime. Due to the particle size distribution the range of charge blocking, below 100 K, is rather wide and overlapping the range where thermal blocking of the paramagnetic relaxation occurs and both effects contribute to the curvature of the *IU* curves. Thus, we did not find the present samples feasible for an extensive investigation of both the voltage and magnetic field dependence at different time scales, as would be required to separate the two effects.

V. SUMMARY AND CONCLUSIONS

This work presents a study of both magnetic and transport properties of thin films comprising discontinuous permalloy ($Ni_{81}Fe_{19}$) layers embedded in aluminum oxide (Al_2O_3). The metal-insulator structure is periodic with well-defined permalloy particles obeying log-normal size distributions. Two films with a nominal thicknesses of the Al_2O_3 layers $t_{\text{oxide}}=16$ Å and a nominal thickness of permalloy $t_{\text{Py}}=6$ Å and $t_{\text{Py}}=8$ Å, respectively, were studied.

Analyses of the magnetic measurements show that the samples comprise ensembles of weakly or noninteracting superparamagnetic particles. The particles are significantly smaller in the sample with the thinner permalloy layers than in that with the thicker ones; displaying log-normal distribution functions with median diameters $D_{\text{med}}=2.8$ nm and 3.1 nm and distribution widths $\sigma_{\text{D}}=1.2$ nm and 1.3 nm, $t_{\text{Py}}=6$ Å and 8 Å, respectively. The superparamagnetic relax-

ation becomes successively blocked below 20 K and 30 K, respectively.

In the electrical resistance measured with the current perpendicular to the film plane, we discern two distinct regimes: (i) the high-temperature regime for $T \geq 100$ K where the resistance is temperature dependent and independent on electric field and (ii) the low-temperature regime for $T < 10$ K where the electric field dependence is prominent and the temperature dependence becomes negligible.

Our results imply that the charge transfer occurs through charges tunneling between the permalloy particles. The energy required for charging of the small particles is obtained from thermal fluctuations at high temperature and from the electric field at low temperature. We applied an effective-medium model for an ensemble of particles with a size distribution to extract the mean charging energy $\langle E_C(d) \rangle \approx 40$ meV at high temperature. The same charging energy was estimated from the gap in the IU curves at 4 K. The polarization of the dielectric matrix and the surrounding metal particles can be accounted for by effective dielectric constants $\epsilon_{\text{eff}} \approx 13$ and 12 for $t_{\text{Py}} = 6$ Å and 8 Å, respectively.

From the electric field dependence of the current at 4 K a scaling parameter in the relation $I \propto (\frac{U}{U_{\text{th}}} - 1)^{\gamma}$, where U_{th} is the threshold for conduction, was estimated to $\gamma \approx 2$ for both films. This value is close to values calculated for two-dimensional systems of charge carriers.

The magnetic field dependence of the resistance reflects the transition from a superparamagnetic state at room temperature, displaying a single maximum of the ratio MR $= [R(B) - R(2\ \text{T})]/R(2\ \text{T})$ in zero field, to a blocked state showing a hysteretic behavior with two split peaks at 4 K. There is a shift between the position of the maxima, amounting to about 0.9% for 6 Å and 1.1% for 8 Å, and the coercive fields of the samples.

ACKNOWLEDGMENTS

Financial support from the Swedish research council (VR) and the Swedish foundation for strategic research (SSF) is acknowledged.

[1] M. N. Baibich, J. M. Broto, A. Fert, F. Nguyen Van Dau, F. Petroff, P. Etienne, G. Creuzet, A. Friederich, and J. Chazelas, Phys. Rev. Lett. **61**, 2472 (1988).
[2] G. Binasch, P. Grünberg, F. Saurenbach, and W. Zinn, Phys. Rev. B **39**, 4828 (1989).
[3] A. E. Berkowitz, J. R. Mitchell, M. J. Carey, A. P. Young, S. Zhang, F. E. Spada, F. T. Parker, A. Hutten, and G. Thomas, Phys. Rev. Lett. **68**, 3745 (1992).
[4] F. Parent, J. Tuaillon, L. B. Stern, V. Dupuis, B. Prevel, A. Perez, P. Melinon, G. Guiraud, R. Morel, A. Barthélémy, and A. Fert, Phys. Rev. B **55**, 3683 (1997).
[5] J. S. Moodera, L. R. Kinder, T. M. Wong, and R. Meservey, Phys. Rev. Lett. **74**, 3273 (1995).
[6] S. Yuasa, T. Nagahama, A. Fukushima, Y. Suzuki, and K. Ando, Nature Mater. **3**, 868 (2004).
[7] S. S. P. Parkin, C. Kaiser, A. Panchula, P. M. Rice, B. Hughes, M. Samant, and S.-H. Yang, Nature Mater. **3**, 862 (2004).
[8] J. I. Gittleman, Y. Goldstein, and S. Bozowski, Phys. Rev. B **5**, 3609 (1972).
[9] L. F. Schelp, A. Fert, F. Fettar, P. Holody, S. F. Lee, J. L. Maurice, F. Petroff, and A. Vaurès, Phys. Rev. B **56**, R5747 (1997).
[10] T. Zhu and Y. J. Wang, Phys. Rev. B **60**, 11918 (1999).
[11] C. T. Black, C. B. Murray, R. L. Sandstrom, and S. Sun, Science **290**, 1131 (2000).
[12] K. Yakushiji, S. Mitani, K. Takanashi, S. Takanashi, and S. Maekawa, Appl. Phys. Lett. **78**, 515 (2001).
[13] H. Sukegawa, S. Nakamura, A. Hirohata, N. Tezuka, and K. Inomata, Phys. Rev. Lett. **94**, 068304 (2005).
[14] For a general review on Coulomb blockade, see L. P. Kouwenhoven, C. M. Marcus, P. L. McEuen, S. Tarucha, R. M. Westervelt, and N. S. Wingreen, in *Mesoscopic Electron Transport*, edited by L. L. Sohn, L. P. Kouwenhoven, and G. Schön (Kluwer, Dordrecht, 1997).
[15] H. Fujimori, S. Ohnuma, N. Kobayashi, and T. Masumoto, J. Magn. Magn. Mater. **304**, 32 (2006).
[16] R. Bručas, M. Hanson, R. Gunnarsson, E. Wahlström, M. van Kampen, B. Hjörvarsson, H. Lidbaum, and K. Leifer, J. Appl. Phys. **101**, 073907 (2007).
[17] R. Bručas and M. Hanson, J. Magn. Magn. Mater. **310**, 2521 (2007).
[18] M. Volmer and A. Weber, Z. Phys. Chem. **119**, 277 (1926).
[19] M. Hanson, C. Johansson, and S. Mørup, J. Phys.: Condens. Matter **7**, 9263 (1995), and references therein.
[20] M. Hanson, C. Johansson, and S. Mørup, J. Phys.: Condens. Matter **5**, 725 (1993).
[21] J. L. García-Palacios, Adv. Chem. Phys. **112**, 1 (2000).
[22] C. A. Neugebauer and M. B. Webb, J. Appl. Phys. **33**, 74 (1962).
[23] A. A. Middleton and N. S. Wingreen, Phys. Rev. Lett. **71**, 3198 (1993).
[24] Ch. Morawe and H. Zabel, J. Appl. Phys. **77**, 1969 (1995).
[25] C. A. F. Fettar, J.-L. Maurice, F. Petroff, L. F. Schelp, A. Vaurès, and A. Fert, Thin Solid Films **319**, 120 (1998).
[26] W. Kleemann, O. Petracic, Ch. Binek, G. N. Kakazei, Yu. G. Pogorelov, J. B. Sousa, S. Cardoso, and P. P. Freitas, Phys. Rev. B **63**, 134423 (2001).
[27] S. Sankar, B. Dieny, and A. E. Berkowitz, J. Appl. Phys. **81**, 5512 (1997).
[28] B. Dieny, S. Sankar, M. R. McCartney, D. J. Smith, P. Bayle-Guillemaud, and A. E. Berkowitz, J. Magn. Magn. Mater. **185**, 283 (1998).
[29] G. N. Kakazei, Yu. G. Pogorelov, A. M. L. Lopes, J. B. Sousa, S. Cardoso, P. P. Freitas, M. M. Pereira de Azevedo, and E. Snoeck, J. Appl. Phys. **90**, 4044 (2001).
[30] M. Anas, C. Bellouard, and M. Vergnat, J. Appl. Phys. **96**, 1159 (2004).
[31] J. B. Sousa, J. A. M. Santos, R. F. A. Silva, J. M. Teixeira, J. Ventura, J. P. Araújo, P. P. Freitas, S. Cardoso, Yu. G. Pogorelov, G. N. Kakazei, and E. Snoeck, J. Appl. Phys. **96**, 3861 (2004).

[32] S. Bedanta, T. Eimüller, W. Kleemann, J. Rhensius, F. Stromberg, E. Amaladass, S. Cardoso, and P. P. Freitas, Phys. Rev. Lett. **98**, 176601 (2007).
[33] H. G. Silva, H. L. Gomes, Y. G. Pogorelov, L. M. C. Pereira, G. N. Kakazei, J. B. Sousa, J. P. Araújo, J. F. L. Mariano, S. Cardoso, and P. P. Freitas, J. Appl. Phys. **106**, 113910 (2009).
[34] A. García-García, A. Vovk, J. A. Pardo, P. Štrichovanec, C. Magén, E. Snoeck, P. A. Algarabel, J. M. De Teresa, L. Morellón and M. R. Ibarra, J. Appl. Phys. **105**, 063909 (2009).
[35] R. Hill, Proc. R. Soc. London, Ser. A **309**, 377 (1969).
[36] P. Sheng and B. Abeles, Phys. Rev. Lett. **28**, 34 (1972).
[37] S. T. Ruggiero and J. B. Barner, Z. Phys. B: Condens. Matter **85**, 333 (1991).
[38] A. Schabowska and J. Szczeklik, Thin Solid Films **75**, 177 (1981).
[39] J. C. Maxwell Garnett, Philos. Trans. R. Soc. London, Ser. A **203**, 385 (1904).
[40] A. K. Gupta and A. K. Sen, Phys. Rev. B **57**, 3375 (1998).
[41] A. J. Rimberg, T. R. Ho, and J. Clarke, Phys. Rev. Lett. **74**, 4714 (1995).
[42] C. Lebreton, C. Vieu, A. Pépin, M. Mejias, F. Carcenac, Y. Jin, and H. Launois, Microelectron. Eng. **41-42**, 507 (1998).
[43] R. P. Tan, J. Carrey, C. Desvaux, L.-M. Lacroix, P. Renaud, B. Chaudret, and M. Respaud, Phys. Rev. B **79**, 174428 (2009).
[44] J. Varalda, W. A. Ortiz, A. J. A. de Oliveira, B. Vodungbo, Y.-L. Zheng, D. Demaille, M. Marangolo, and D. H. Mosca, J. Appl. Phys. **101**, 014318 (2007).